A Novel Diagnosis and Location Method of Short-Circuit Grounding High-Impedance Fault for a Mesh Topology Constant Current Remote Power Supply System in Cabled Underwater Information Networks

ZHENG ZHANG [ORCID], XUEJUN ZHOU, XICHEN WANG, AND LEI WANG

College of Electronic Engineering, Naval University of Engineering, Wuhan 430033, China

Corresponding author: Xichen Wang (hjgcwxc@163.com)

ABSTRACT Cabled underwater information networks (CUINs) have evolved over the last decade to provide abundant power and broad bandwidth communication to enable marine science. To ensure reliable operation of CUINs, it is essential to have the technology for high-impedance fault diagnosis and isolation with high reliability and accuracy. The short-circuit grounding high-impedance fault status of mesh topology constant current remote supply system was diagnosed by analyzing the variation difference of equivalent current in the Laplace transform domain. Shore power feeding equipment (SPFE) supplied the power for underwater system individually from both terminals, and the fault location was located by calculating the shunt loss of the current in the trunk before and after the fault. Thus, the fault was isolated to maintain normal operation of the rest of the system and improve the reliability of CUINs. According to the established typical mesh topology constant current remote supply system circuit model, the fault location scheme was designed to simulate the faults of the cable sections in the different links in the constant current remote supply system, and the changes of current located at the primary nodes (PNs) in the Laplace transform domain before and after the fault were analyzed. The results show that the equivalent current of each PN changes when a fault occurs in the system, and the location of the fault point can be analyzed by comparing the shunt loss of the current in the trunk before and after the fault. The designed method of short-circuit grounding high-impedance fault diagnosis and location for a constant current remote supply system is suitable for the fault monitoring and judgment of CUINs with high feasibility and practicality. Furthermore, it provides technical support for the resulting effective determination of faults, isolation of faults, protection of equipment, and improvement of the system reliability.

INDEX TERMS Cabled underwater information networks (CUINs), constant current, short-circuit grounding high-impedance fault, fault diagnosis, point location, reliability.

I. INTRODUCTION

Approximately 70% of the earth is covered by ocean. Exploring the operating mechanism of the deep ocean is the key to understanding the development of human civilization [1]–[4]. Over the last several decades, the observation of the ocean with traditional shipborne and airborne mobile platforms,

The associate editor coordinating the review of this article and approving it for publication was Yan-Jun Liu.

exploration by battery-powered instruments [5], underwater unmanned vehicles (UUVs) [6]–[8], anchors or buoys, satellite telemetry and other technological approaches have only explored and researched the changes of the shallow ocean in a one-sided, sporadic, intermittent manner. These approaches have limited perspectives and concepts connected to oceanic observation, understanding and development. To explore and understand the ocean and promote the development of marine science [9], [10], the marine science community has proposed

a third platform for observing the ocean [11], that is, cabled underwater information networks (CUINs).

CUINs have eliminated the limitations of time and space in marine research methods such as shore-based fixed platforms, shipborne and airborne mobile platforms, and satellite remote sensing telemetry, which are able to satisfy the needs for long-term, real-time, and all-weather observation of the ocean [12], [13]. Various instruments and equipment are placed on the seafloor, which are supplied with submarine cable networks connected to shore power feeding equipment (SPFE) [14]. Therefore, the performance of the remote power supply system determines whether the CUINs can operate normally. Currently, there are two major types of power supply systems used internationally and both are direct current (DC). In the first type, the trunk cable operates at a nominally constant voltage (CV) [15] and all nodes are parallel connected using seawater as a return; some examples of these systems are the North East Pacific Time-Integrated Undersea Networked Experiments (NEPTUNE- Canada) [16], [17] and other operating systems [18], [19]. In the second type, the trunk cable operates in a constant current (CC) mode [14]. Flowing through isolated-type high-frequency switching constant current/constant current converters (CC/CC) in primary nodes (PNs), the electrical energy is branched and provides a constant current power supply to the electrical equipment mounted on the secondary nodes (SNs) in a branch cable; an example of these systems is the Dense Ocean Network for Earthquakes and Tsunamis (DONET) [20], [21]. The system using the CC mode has good self-healing properties that protect against short-circuit grounding faults (parts of the system can continue to operate through a fault, and the system does not need a high-medium-low voltage conversion [22], which has the advantages of modularization and standardization of the power conversion module. The CC mode appears to be somewhat favored for more general, purpose-built, science-driven observatories [14], [21].

The operation of the remote power supply system cannot avoid the faults caused by human damage and changes in the geographical environment.

Therefore, no matter what kind of remote power supply system mode is applied, the fault location and isolation are keys to the operation and maintenance of the system. The constant current remote power supply system in CUINs is different from backbone optical network and power distribution network on land. Currently, the fault location of CUINs is a big problem in the field of ocean engineering, and there is no clear definition and criterion yet. Currently, fault monitoring and diagnosis of cable system underwater information network at home and abroad mainly uses distributed optical fiber sensing system and insulating conductor testing methods. In 1995, Hirohumi T. *et al.* [23], [24] used distributed optical fiber sensors to monitor the temperature change and breakdown of 6.6 kV submarine cable cores. In 1997, 400 kV submarine cables connecting Jordan and Egypt, the Raman scattering distributed optical fiber temperature was firstly used to monitor the temperature changes inside the cables [106]. The optical fiber sensing Hull support system developed by Future Fiber Technology Company [25] utilized laser interference principle and optical fiber sensing network to realize the functions of moving, vibration induction, micro-strain detection and positioning of submarine cables. Natu [26] proposed an adaptive detection algorithm, which uses the smallest number of detection stations to achieve fault diagnosis and location. Literature [27] stated that the traditional cable detection methods mainly include insulation resistance comparison method. Currently, there is very little research on fault diagnosis and location for the underwater DC power supply system [28]. Wang Y. *et al.* proposed a novel preliminary-summation-based principal component analysis (PS-PCA) method to cope with the combined Gaussian and non-Gaussian features in the fault detection processes [29], and Multivariate statistical process monitoring (MSPM) methods, which are significant for improving production efficiency and enhancing safety, are proposed [30]. Chen Y. *et al.* proposed an actively controllable method which configures each branch link of the network [19] by changing the input current of the SPFE, and constant voltage is employed to locate the system fault by using the measured voltage current and impedance method; n this way, a relevant laboratory experimental prototype was designed. Lu S., Chan T. *et al.* proposed a method directed against the short/open-circuit faults of the constant voltage remote power supply system in the NEPTUNE observation network [20], [31] by changing the polarity of the SPFE output voltage; the links for the power and communication in the branching unit (BU) are adjusted to control the interrupter switching and to determine the short-circuit fault location and isolation. Chan T. *et al.* designed a constant voltage-constant current (CV-CC) hybrid fault detection system [32] for open-circuit faults in constant voltage remote power supply systems. Zhang Z. *et al.* reviewed the advantages and disadvantages of existing switching methods and proposed a novel active switching method for the network configuration, which provides a way to communicate with the shore station (SS) through an existing power transmission path [33]. Lyu F. *et al.* [34], [35] summarized the typical topology of the CUINs based on the controllability of the electrical switching BU and the power monitoring and control system (PMACS) and communications monitoring and control system (CMACS), with a new method for the open-circuit fault location of the submarine cable proposed by analyzing the weighted least squares status estimation formula of the branching unit (BU) node voltage vector. According to the generalized Kirchhoff's current law (KCL), the method based on the leakage current error vector generated by the open-circuit fault in the constant voltage remote power supply system was proposed [36]. An active node fault switching and isolating method based on a discrete-voltage intervention is proposed and aimed at controlling a specific node inserted in or cut away from the whole underwater network [37]. Zheng S. *et al.* proposed an HVDC power switching circuit
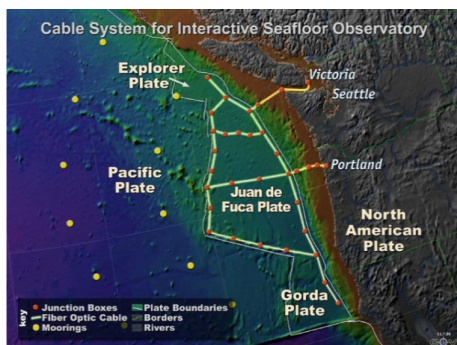
FIGURE 1. The design structure of the North East Pacific time-integrated undersea networked experiments (NEPTUNE-Canada), a typical mesh topology cabled underwater information network.

for the BUs of CUINs based on the voltage sharing scheme of the series-connected IGBTs [38]. Zhang F. *et al.* mainly analyzed the reason for the short fault and discussed the different methods to isolate the short part in a different location in the CV mode [39], [40]. However, for a constant current remote power supply system, a short-circuit fault will cause damage to the remote transmission capability of the system, but it will not cause the system to stop operating. Overall, an open-circuit fault will result in an excessive surge voltage and may even cause the system to collapse. However, for a constant current remote power supply system, a low-impedance fault will cause damage to the remote transmission capability of the system, but it will not cause the system to stop operating. However, a high-impedance fault will result in an excessive surge voltage and may even cause the system to collapse. Currently, the research on fault switching protection of remote power supply system for CUINs is still in its infancy stage, and there are few studies on the diagnosis and location of the short-circuit grounding high-impedance fault status for a constant current power supply system due to the blockade restrictions of power conversion technology in underwater constant current remote power supply systems.

In this paper, theoretical research was conducted on the short-circuit grounding high-impedance fault diagnosis and localization of mesh topology constant current remote supply system in CUINs. Based on the equivalent principle of the Norton current source, a fault diagnosis method for short-circuit grounding high-impedance faults is proposed by analyzing the variation difference of the equivalent current at each PN in the Laplace transform domain, and the accurate location of short-circuit grounding high-impedance fault point by the method of bidirectional detection from the SS of shunt loss of the current in the trunk, which provides technical support for subsequent effective judgment, isolation of faults, protection of equipment, and improvement of system robustness.

II. ESTABLISHMENT OF THE MODEL FOR THE MESH TOPOLOGY CONSTANT CURRENT REMOTE POWER SUPPLY SYSTEM

The constant current remote power supply system is one of the DC power supply systems, which transmits and distributes

(a)
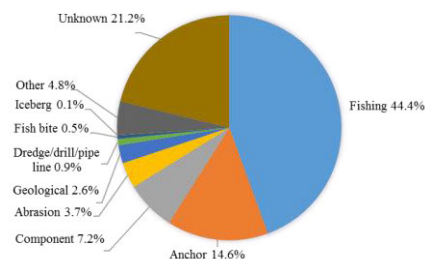
(b)

FIGURE 2. The global summary chart of the cable fault caused by the external damage in the last 50 years: (a) the distribution map of the 2162 cases of the cable fault caused by external forces by 2006; (b) proportion of cable faults by cause.
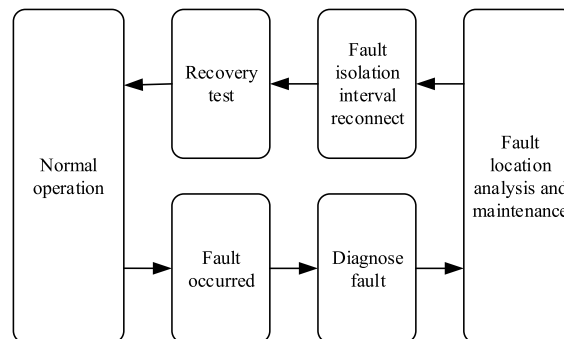

FIGURE 3. Schematic diagram of the operation and maintenance of a constant current remote power supply system.

power from the SPFE to underwater facilities through remote submarine cables (typically hundreds of km) with a seawater return. The NEPTUNE-Canada, a typical mesh topology for a cabled underwater information network, is depicted in Figure 1.

Based on the data [19] provided by Tyco Communications Corporation, fisheries and other marine activities are currently frequent, and with the rapid development of science and technology, fishing boats can now fish in waters with a depth of 1500 m. Due to the lack of appropriate management and mechanism operation, cable damage has occurred in most sea areas. A total of 2162 cases of cable fault was caused by external forces by 2006, which are illustrated in Figure 2(a) and (b). Therefore, the research on fault diagnosis and location of the underwater remote supply system is the most important task in the construction of CUINs. In the operating process for the constant current remote power supply
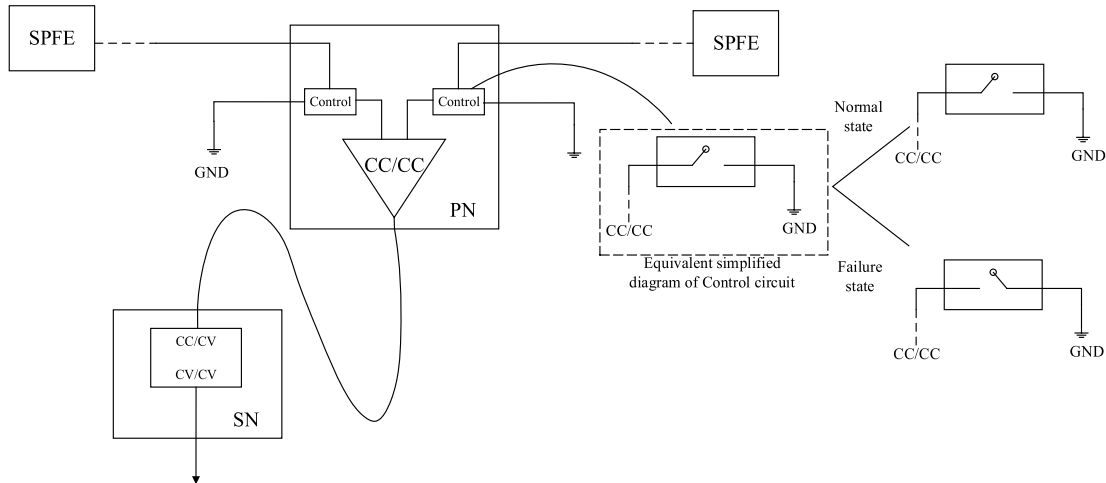
FIGURE 4. Schematic diagram of the isolating high-impedance fault in constant current remote power supply system.

system and according to the property of the fault, the faults can be divided into short-circuit faults and open-circuit faults. When the conductive medium in the system has a connection fault, the location of the fault is equivalent to hundreds or even several megabytes of resistance, which results in open-circuit faults in the system. In contrast, when a certain damaged point in the network is grounded with seawater as a return, which results in a short-circuit fault in the system.

If a short-circuit fault occurs, the power supply conductor at the short-circuit grounding point forms a return circuit with seawater and produces an anode or cathode in which the metal at the anode terminal gradually decreases due to seawater electrical corrosion and continuously consumes the power supply conductor of the cable. Meanwhile, bubbles are generated at the immersed grounding point, which results in the reduction of the contact area between the conductor and seawater, and increase of equivalent resistance, or even isolation that turns into an open-circuit fault status. Then, the circuit is blocked, which results in the interruption of power supply in the whole system. The number of conductive ions in different water is different. Sometimes, the equivalent resistance of short-circuit fault points forms the ground high impedance, which cannot eliminate the shunt effect. Therefore, once the fault occurs, a diagnostic analysis should immediately be performed, the fault point determined, and the fault section isolated as soon as possible, to ensure normal operation of the rest. Subsequently, the fault isolation section should be reconnected to the remote power supply system after maintenance at the fault location. Then, the system should operate normally in the recovery test. The operation and maintenance of a constant current remote power supply system is illustrated in Figure 3.

The main power supply equipment in PNs are CC/CC converters and constant current/constant voltage (CC/CV) converters. The main equipment in SNs are CC/CV converters and constant voltage/ constant voltage (CV/CV) converters. As shown in Figure 4, the controller can be set in the PNs
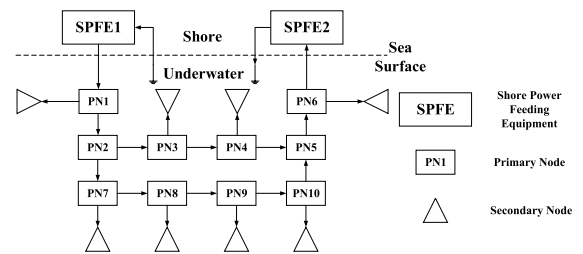

FIGURE 5. Model of the two-terminal 10-node mesh topology constant current remote power supply system in CUINs.

to ensure that the fault is isolated. When a high-impedance fault occurs in the trunk cables, the fault signal reacts to the neighboring PNs, whereas the controllers in the PN make judgments by analysis and comparison. When the system determines that a high-impedance signal has occurred, the controllers automatically switch to the ground terminal to form a new circuit ensuring that the rest of the system can still operate normally with the fault section insulated.

Figure 5 shows the model of the typical two-terminal 10-node mesh topology constant current remote power supply system in the CUINs, where the constant current remote power supply system forms a return circuit using seawater. Because the PNs and SPFE in the trunk cables have current flow directions, according to analysis of the variation difference of equivalent current in the Laplace transform domain, the fault can be diagnosed and located.

According to the KCL and the Kirchhoff's voltage law (KVL), in the circuit, the sum of the voltage algebra in any closed circuit constant to zero based on the topological structure of the constant current remote supply system, and the current at the PN can be measured by the detection device in the junction box [41].

The power supply conductor in the core of the submarine cable is a mixed conductor composed of special conductive copper tube (or copper wire) and other metals, which are also a mixed conductor composed of distributed inductance,
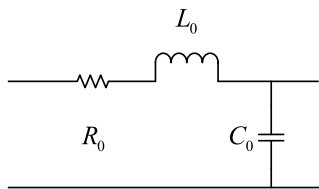
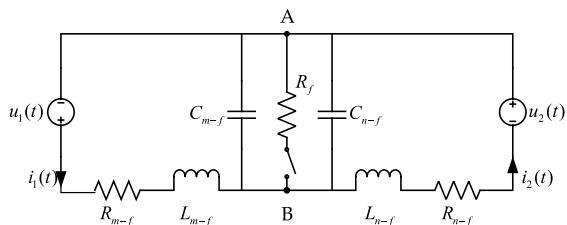**FIGURE 6.** Schematic diagram of the equivalent circuit of the submarine cable.

FIGURE 7. Schematic diagram of an equivalent circuit between node PN-*m* and PN-*n*.

capacitance and resistance. When the input is DC, the cable can be simplified to pure resistance, however, the distributed inductance and capacitance in the system must be considered when the current generates impulse feedback. The equivalent circuit of submarine cable is shown in Figure 6, where,,, and are the distributed capacitance, inductance, and resistance of the cable.

Based on the equivalent principle of the Norton current source [42], the equivalent analysis of the adjacent PN-*m* and PN-*n* is conducted is depicted in Figure 7, where $i_1(t)$ and $i_2(t)$ are equivalent output currents of constant current sources on both sides of the PN-*m* and PN-*n*; $u_1(t)$ and $u_2(t)$ are equivalent output voltages of the constant current sources on both sides of the PN-*m* and PN-*n*; R_{m-f}, L_{m-f}, and C_{m-f} are the equivalent resistance, inductance and capacitance from PN-*m* to the fault point f; R_{n-f}, L_{n-f} and C_{n-f} are the equivalent resistance, inductance and capacitance from PN-*n* to the fault point f; and R_f is the equivalent resistance to ground at the fault point f.

If no fault occurs, the fault switch in Figure 7 can be disconnected. Then, the circuits can be analyzed equivalently from both terminals, which are illustrated in the Figure 8(a) and (b), where $i_{C1}(t)$ and $i_{C2}(t)$ are currents flowing through capacitor C_{m-n}; $i_{L1}(t)$ and $i_{L2}(t)$ are currents flowing through inductors L_{n-f} and L_{m-f} when they are powered by both terminals respectively.

As shown in Figure 8(a), according to the KCL, the relationship between the distributed capacitance, inductance and the equivalent power supply $u_1(t)$ flowing through the normal operation can be obtained

$$\begin{cases} R_{m-f}i_1(t) + L_{m-f}\dfrac{d}{dt}i_1(t) + \dfrac{1}{C_{m-n}}\displaystyle\int_{0_-}^{t} i_{C1}(\tau)dt = u_1(t) \\ u_{C1}(t) = \dfrac{1}{C_{m-n}}\displaystyle\int_{0_-}^{t} i_{C1}(\tau)dt = L_{n-f}\dfrac{d}{dt}i_{L1}(t) + R_{n-f}i_{L1}(t) \\ i_1(t) = i_{C1}(t) + i_{L1}(t) \end{cases} \tag{1}$$
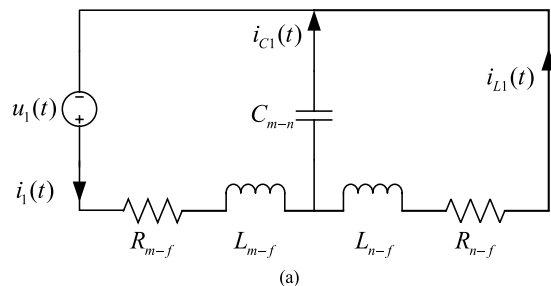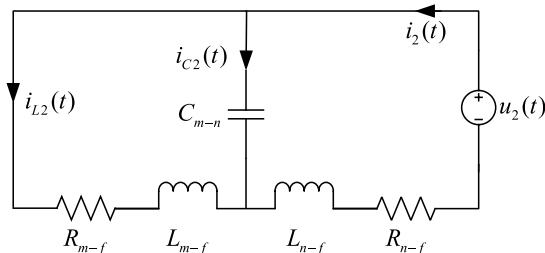
FIGURE 8. Schematic diagram of the equivalent circuit under normal operating conditions.(a) Schematic diagram of the left- terminal SPFE power supply equivalent circuit. (b) Schematic diagram of the right-terminal SPFE power supply equivalent circuit.

Adjusting (1) and eliminating variable parameter $i_{L1}(t)$, we get;

$$\begin{cases} i_{L1}(t) = i_1(t) - i_{C1}(t) \\ \dfrac{1}{C_{m-n}}\displaystyle\int_{0_-}^{t} i_{C1}(\tau)dt = L_{n-f}\dfrac{d}{dt}i_1(t) - L_{n-f}\dfrac{d}{dt}i_{C1}(t) \\ \quad + R_{n-f}\left[i_1(t) - i_{C1}(t)\right] \end{cases} \tag{2}$$

The relationship between the current $i_{C1}(t)$ flowing through the distributed capacitor and the equivalent input current $i_1(t)$ is obtained;

$$\frac{1}{C_{m-n}}i_{C1}(t) + L_{n-f}\frac{d^2}{dt^2}i_{C1}(t) + R_{n-f}\frac{d}{dt}i_{C1}(t)$$
$$= L_{n-f}\frac{d^2}{dt^2}i_1(t) + R_{n-f}\frac{d}{dt}i_1(t) \tag{3}$$

Similarly, as shown in Figure 8(b), the relationship between the distributed capacitance, inductance and the equivalent power supply $u_2(t)$ flowing through normal operation can also be obtained;

$$\begin{cases} R_{n-f}i_2(t) + L_{n-f}\dfrac{d}{dt}i_2(t) + \dfrac{1}{C_{m-n}}\displaystyle\int_{0_-}^{t} i_{C2}(\tau)dt = u_2(t) \\ u_{C2}(t) = \dfrac{1}{C_{m-n}}\displaystyle\int_{0_-}^{t} i_{C2}(\tau)dt = L_{n-f}\dfrac{d}{dt}i_{L2}(t) + R_{n-f}i_{L2}(t) \\ i_2(t) = i_{C2}(t) + i_{L2}(t) \end{cases} \tag{4}$$

Eliminating the variable parameter $i_{L2}(t)$, and when the relationship between the current $i_{C2}(t)$ flowing through the distributed capacitor and the equivalent input current $i_2(t)$ is obtained;

$$\frac{1}{C_{m-n}}i_{C2}(t) + L_{m-f}\frac{d^2}{dt^2}i_{C2}(t) + R_{m-f}\frac{d}{dt}i_{C2}(t)$$
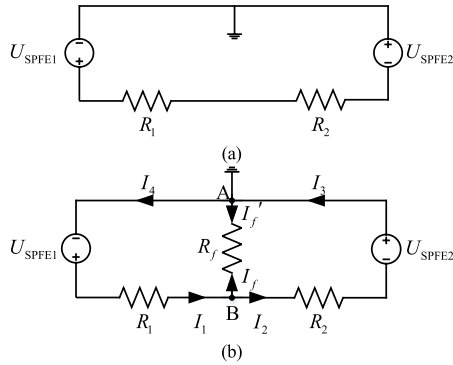
FIGURE 9. Schematic diagram of the system equivalent circuit in the stable status. (a) Normal operational status. (b) Fault status.

$$= L_{m-f}\frac{\mathrm{d}^2}{\mathrm{d}t^2}i_2(t) + R_{m-f}\frac{\mathrm{d}}{\mathrm{d}t}i_2(t) \quad (5)$$

When the circuit is stable and according to the constant current characteristic;

$$i_1(t) = i_2(t) \quad (6)$$

Substituting (6) into (3) and (5), the relationship of the current on the capacitance C_{m-n} in the situation where the power supply from both terminals is obtained;

$$\frac{1}{C_{m-n}}i_{C1}(t) + L_{n-f}\frac{\mathrm{d}^2}{\mathrm{d}t^2}i_{C1}(t) + R_{n-f}\frac{\mathrm{d}}{\mathrm{d}t}i_{C1}(t)$$
$$= \frac{1}{C_{m-n}}i_{C2}(t) + L_{m-f}\frac{\mathrm{d}^2}{\mathrm{d}t^2}i_{C2}(t) + R_{m-f}\frac{\mathrm{d}}{\mathrm{d}t}i_{C2}(t) \quad (7)$$

As shown in Figure 6, the current equations of nodes A and B can be listed based on KCL;

$$\begin{cases} i_1(t) = i_{C1}(t) + i_2(t) \\ i_2(t) = i_{C2}(t) + i_1(t) \end{cases} \quad (8)$$

The system supplies the DC constant current source, Substituting (8) into (7);

$$i_{C1}(t) = i_{C2}(t) = 0 \quad (9)$$

When the constant current remote supply system is in the normal or fault status, the input DC constant current of the SS is stable. Meanwhile, the distributed capacitance and inductance of the cable without the voltage load, which can be equivalently ignored, is shown in Figure 9(a) and (b).

where, I_1, I_2, I_3, I_4 and I_f, I_f' are the currents in the links of the circuit and the currents passing through the fault points, respectively; R_1 and R_2 are the equivalent loads of the system at both terminal s of the fault.

Because SPFE1 and SPFE2 are constant current sources, when a fault occurs, to maintain the constant current characteristics of the constant current source;

$$I_1 = I_2, \quad I_3 = I_4 \quad (10)$$

According to KCL, the current equation of node A is;

$$I_3 = I_4 + I_f' \quad (11)$$

Substituting (11) into (10), $I_f' = 0$ can be obtained.

Similarly, according to the KCL equation of node B, $I_f = 0$ can be obtained. Meanwhile, the current flowing through the fault point f is zero and there is no current at the fault point.

In summary, no current flows through the capacitor when the system is in normal and stable operational status. Meanwhile, when the short-circuit grounding high-impedance fault occurs in the constant current remote power supply system, the circuit will change instantaneously. However, the SPFEs maintain the constant current power supply characteristics of the system, the SPFE self-adjusts the fault, and there is no current flowing through the equivalent resistance at the fault point. In addition, the stable fault point will not lose the power supply, which is the fault self-healing of the constant current remote power supply system. There is no voltage difference between the fault point and the ground terminal of the SPFE, while the fault point is not easy to detect, which also results in difficulties for fault detection and diagnosis. Therefore, a short-circuit grounding high-impedance fault diagnosis and identification method by analyzing the difference of equivalent current variation in the Laplace transform domain at each PN is proposed in this paper. The fault location is determined by calculating the shunt loss of the current in the trunk before and after the fault by supplying individually from both terminals of SPFE.

III. ANALYSIS OF SHORT-CIRCUIT GROUNDING HIGH-IMPEDANCE FAULT LOCATION FOR A CONSTANT CURRENT REMOTE POWER SUPPLY SYSTEM

When a fault occurs in the branch cable, the load voltage of the PN changes significantly, and even the overload protection of the PN will cause no valid data upload and the measured voltage of the SN will change. Therefore, it is possible to diagnose short-circuit grounding high-impedance fault in the branch cable by measuring the significant change of the voltage in the trunk and the data feedback from the information acquisition equipment.

However, the diagnosis and location of the short-circuit grounding high-impedance fault in the trunk cable is different from that in the branch cable. It is impossible to locate the fault directly by observing the data. The seabed environment is complex and changeable, whereas the submarine cable may be bent, pulled, torn or broken due to fishing, anchoring, seabed earthquakes and mudslides, which cause the cable insulation to break down and form the grounding fault. If the trunk cable breaks in full contact with the seawater to form a return circuit, the seawater (as a good conductor) is equivalent to a non-resistive conductor or a few resistances, the system can diagnose the short-circuit low-level impedance fault status by analyzing the directional matrix of the current flow direction and the mean error value. When the number of conductive ions in water is small or the anode loss resistance increases due to the mistaken diagnosis of short-circuit low-level impedance fault, then it needs to be re-analyzed.

Assuming that there is short-circuit grounding high-impedance fault between PN-m and PN-n, the switch in Figure 6 is closed. The capacitive inductance between PN-m
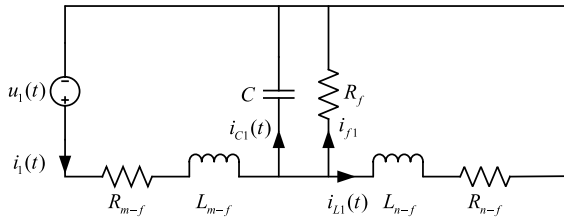
FIGURE 10. Equivalent circuit diagram of the left- terminal SPFE power supply after fault occurs.

FIGURE 11. Equivalent circuit diagram of the right- terminal SPFE power supply after fault occurs.

and PN-n will react to the system. The equivalent circuit diagram of the left- terminal SPFE power supply after fault power supply analysis is performed by the left- terminal SPFE, as shown in Figure 10.

According to the KCL, the current flowing through the equivalent resistance at the fault point is obtained;

$$i_f(t) = \frac{L_{n-f}\frac{d}{dt}i_L(t) + R_{n-f}i_L(t)}{R_f} \quad (12)$$

As shown in Figure 10, based on the circuit form, the circuit equation of the circuit can be obtained;

$$\begin{cases} u_1(t) = R_{m-f}i_1(t) + L_{m-f}\frac{d}{dt}i_1(t) + u_C(t) \\ u_C(t) = \frac{1}{C}\int_{-\infty}^{t} i_C(\tau)d\tau = L_{n-f}\frac{d}{dt}i_L(t) + R_{n-f}i_L(t) \\ i_1(t) = i_C(t) + i_L(t) + i_f(t) \end{cases} \quad (13)$$

Eliminating the variable parameter $u_C(t)$ in (13);

$$\int_{-\infty}^{t} i_1(\tau)d\tau = CL_{n-f}\frac{d}{dt}i_L(t) + CR_{n-f}i_L(t)$$
$$+ \int_{-\infty}^{t} i_L(\tau)d\tau + \int_{-\infty}^{t} i_f(\tau)d\tau \quad (14)$$

$$u_1(t) = R_{m-f}i_1(t) + L_{m-f}\frac{d}{dt}i_1(t) + \frac{1}{C}\int_{-\infty}^{t} i_1(\tau)d\tau$$
$$- \frac{1}{C}\int_{-\infty}^{t} i_L(\tau)d\tau - \frac{1}{C}\int_{-\infty}^{t} i_f(\tau)d\tau \quad (15)$$

Combining (13), (14), and (15), the relationship among input current and current shunting through the fault can be obtained;

$$\frac{d}{dt}u_1(t) = R_{m-f}\frac{d}{dt}i_1(t) + L_{m-f}\frac{d^2}{dt^2}i_1(t)$$
$$+ \frac{1}{C}i_1(t) - \frac{1}{C}i_L(t) - \frac{1}{C}i_f(t) \quad (16)$$

$$u_1(t) = R_{m-f}i_1(t) + L_{m-f}\frac{d}{dt}i_1(t)$$
$$+ L_{n-f}\frac{d}{dt}i_L(t) + R_{n-f}i_L(t) \quad (17)$$

Substituting (17) into (16), and Eliminating the variable parameter $u_1(t)$;

$$R_{m-f}\frac{d}{dt}i_1(t) + L_{m-f}\frac{d^2}{dt^2}i_1(t) + \frac{1}{C}i_1(t) - \frac{1}{C}i_L(t) - \frac{1}{C}i_f(t)$$
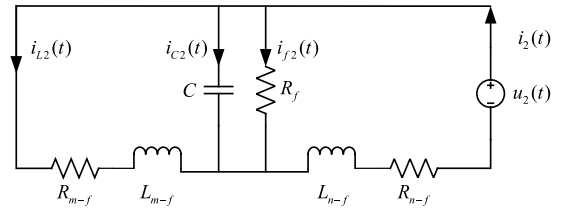
$$= R_{m-f}\frac{d}{dt}i_1(t) + L_{m-f}\frac{d^2}{dt^2}i_1(t)$$
$$+ L_{n-f}\frac{d^2}{dt^2}i_L(t) + R_{n-f}\frac{d}{dt}i_L(t) \quad (18)$$

By substituting (12) into (18), and eliminating the variable parameter $i_f(t)$, the relationship between the input current of the system $i_1(t)$ and the current $i_L(t)$ flowing through the trunk inductance L_{n-f} can be obtained;

$$\frac{1}{C}i_1(t) - \frac{1}{C}i_L(t) - \frac{L_{n-f}\frac{d}{dt}i_L(t) + R_{n-f}i_L(t)}{CR_f}$$
$$= L_{n-f}\frac{d^2}{dt^2}i_L(t) + R_{n-f}\frac{d}{dt}i_L(t) \quad (19)$$

Laplacian transformation of (19);

$$\frac{1}{C}i_1(s) - \frac{1}{C}i_L(s) - \frac{L_{n-f}}{CR_f}si_L(s) - \frac{L_{n-f}}{CR_f}i_L(s)$$
$$= L_{n-f}s^2i_L(s) + R_{n-f}si_L(s) \quad (20)$$

Sorting out (20) and the result is shown;

$$i_L(s) = \frac{1}{CL_{n-f}s^2 + \left(CR_{n-f} + \frac{L_{n-f}}{R_f}\right)s + \left(1 + \frac{R_{n-f}}{R_f}\right)}i_1(s) \quad (21)$$

When the short-circuit grounding high-impedance fault occurs, the current at both terminals of capacitor and inductor will not change abruptly;

$$\begin{cases} i_C(0_+) = i_C(0_-) \\ i_L(0_+) = i_L(0_-) \end{cases} \quad (22)$$

When the system has a fault and assuming that the equivalent input current of the system $i_1(t)$ is an excitation response, the SPFE supply will not change abruptly. Supposing $i_1(s)$ is a constant value α, when $t = 0_+, s = 0$;

$$i_L(s) = \frac{R_{n-f}}{R_{n-f} + R_f}\alpha \quad (23)$$

As shown in Figure 11, according to the KCL, the current flowing through the equivalent resistance, which is supplied by the right- terminal SPFE, at the fault point is obtained;

$$\begin{cases} i_2(t) = i_C(t) + i_L(t) + i_f(t) \\ u_2(t) = R_{n-f}i_2(t) + L_{n-f}\frac{d}{dt}i_2(t) + u_C(t) \\ u_C(t) = \frac{1}{C}\int_{-\infty}^{t} i_C(\tau)d\tau = L_{m-f}\frac{d}{dt}i_L(t) + R_{m-f}i_L(t) \end{cases} \quad (24)$$
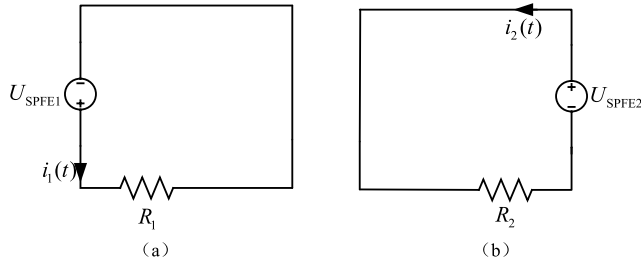
FIGURE 12. Equivalent schematic diagram of the equal power supply after fault. (a) The left-terminal equivalent circuit. (b) The right- terminal equivalent circuit.

Similarly, the relationship between the input current of the system $i_2(t)$ and the current $i_L(t)$ flowing through the trunk inductance L_{m-f} can be obtained;

$$\frac{1}{C}i_2(t) = L_{m-f}\frac{d^2}{dt^2}i_L(t) + \left(\frac{L_{m-f}}{CR_f} + R_{m-f}\right)\frac{d}{dt}i_L(t)$$
$$+ \left(\frac{1}{C} + \frac{R_{m-f}}{CR_f}\right)i_L(t) \quad (25)$$

Laplacian transformation of (25);

$$i_L(s) = \frac{1}{CL_{m-f}s^2 + \left(\frac{L_{m-f}}{R_f} + CR_{m-f}\right)s + \left(1 + \frac{R_{m-f}}{R_f}\right)}i_2(s) \tag{26}$$

When the system has a fault and assuming that the equivalent input current of the system $i_2(t)$ is an excitation response, the SPFE supply will not change abruptly. Supposing $i_2(s)$ is a constant value β, when $t = 0_+$, $s = 0$;

$$i_L(s) = \frac{R_{m-f}}{R_{m-f} + R_f}\beta \tag{27}$$

As shown in Figure 7(b), node A and node B have zero potential equivalents, the circuit after the fault can be equivalent to two circuits supplied by two- terminal SPFE, which are depicted in Figure 12.

The output voltage values of SPFE1 and SPFE2 can be obtained by the return circuit;

$$\begin{cases} U_{\text{SPFE1}} = i_1(t)R_1 \\ U_{\text{SPFE2}} = i_2(t)R_2 \end{cases} \tag{28}$$

As shown in Figure 12(a), when the system operates normally, the SPFE with the two-terminal power supply has the characteristics of constant current and voltage sharing;

$$U_{\text{SPFE1-original}} = U_{\text{SPFE2-original}} = \frac{R_1 + R_2}{2}i_1(t) \tag{29}$$

From (28) and (29), it is clear that the load amount of SPFE1 and SPFE2 changes, and the voltage changes accordingly, that is, there is a fault.

By Combining with (23), (27), and (29) and analyzing the variation difference of equivalent current in the Laplace transform domain, it is possible to diagnose the interval of short-circuit grounding high-impedance fault and the fault status of the constant current remote supply system

short-circuit grounding high-impedance fault. However, this method can't accurately locate the fault. Therefore, this paper adopts the method of separately supplying power from both terminal SPFEs, and locates the short-circuit fault point by calculating the current shunt loss before and after the fault.

The power is supplied by SPFE1 and SPFE2 individually, because the fault interval has been determined. Thus, assuming that the fault occurs between PN-*m* and PN-*n*, the fault location analysis of the system is conducted, as shown in Figure 12, where the R_m and R_m are the equivalent impedances of the PN-*m* and PN-*n* to the SS in the fault state; R_{m-f} and R_{n-f} are the equivalent impedances of the nodes PN-*m* and PN-*n* to the fault point f in the fault state; I_1 to I_6 is the value current of each link in the power supply return circuit.

As shown in Figure 13(a) and (b), the circuit equation of the circuit can be obtained;

$$\begin{cases} I_1 = I_2 + I_3 \\ R_{m-n} = R_{m-f} + R_{n-f} \\ I_2R_f = I_3\left(R_n + R_{n-f}\right) \\ U_{\text{SPFE1}} = I_1\left(R_m + R_{m-f}\right) + I_2R_f \end{cases} \tag{30}$$

$$\begin{cases} I_4 = I_5 + I_6 \\ R_{m-n} = R_{m-f} + R_{n-f} \\ I_5R_f = I_6\left(R_{m-f} + R_m\right) \\ U_{\text{SPFE2}} = I_6\left(R_m + R_{m-f}\right) + I_5R_f \end{cases} \tag{31}$$

Sorting out (30) and (31), the result is shown as;

$$\begin{cases} R_{m-f} = \dfrac{U_{\text{SPFE1}} - I_1R_m - I_3\left(R_n + R_{m-n}\right)}{I_1 - I_3} \\ \quad = \dfrac{I_6R_m + I_4\left(R_n + R_{m-n}\right) - U_{\text{SPFE2}}}{I_4 - I_6} \\ R_{n-f} = \dfrac{I_1\left(R_m + R_{m-n}\right) + I_3R_n - U_{\text{SPFE1}}}{I_1 - I_3} \\ \quad = \dfrac{U_{\text{SPFE2}} - I_6\left(R_m + R_{m-n}\right) - I_4R_n}{I_4 - I_6} \\ R_f = \dfrac{I_1I_3\left(R_n + R_m + R_{m-n}\right) - I_3U_{\text{SPFE1}}}{(I_1 - I_3)^2} \\ \quad = \dfrac{I_4U_{\text{SPFE2}} - I_4I_6\left(R_n + R_m + R_{m-n}\right)}{(I_4 - I_6)^2} \end{cases} \tag{32}$$

The power supply detection value at both terminals is averaged to obtain the resistance value at the fault;

$$\begin{cases} R_{m-f} = \left(\begin{array}{l} \dfrac{U_{\text{SPFE1}} - I_1R_m - I_3\left(R_n + R_{m-n}\right)}{I_1 - I_3} \\ + \dfrac{I_6R_m + I_4\left(R_n + R_{m-n}\right) - U_{\text{SPFE2}}}{I_4 - I_6} \end{array}\right)/2 \\ R_{n-f} = \left(\begin{array}{l} \dfrac{I_1\left(R_m + R_{m-n}\right) + I_3R_n - U_{\text{SPFE1}}}{I_1 - I_3} \\ + \dfrac{U_{\text{SPFE2}} - I_6\left(R_m + R_{m-n}\right) - I_4R_n}{I_4 - I_6} \end{array}\right)/2 \\ R_f = \left(\begin{array}{l} \dfrac{I_1I_3\left(R_n + R_m + R_{m-n}\right) - I_3U_{\text{SPFE1}}}{(I_1 - I_3)^2} \\ + \dfrac{I_4U_{\text{SPFE2}} - I_4I_6\left(R_n + R_m + R_{m-n}\right)}{(I_4 - I_6)^2} \end{array}\right)/2 \end{cases} \tag{33}$$
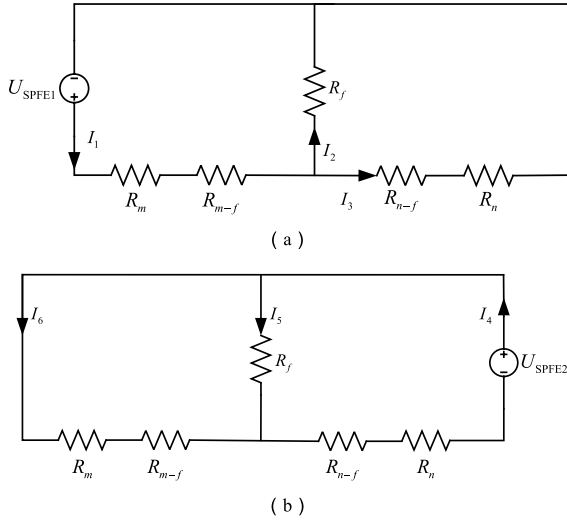
FIGURE 13. Equivalent schematic diagram of equal power supply after fault. (a) The equivalent circuit supplied by the left- terminal SPFE. (b) The equivalent circuit supplied by the right- terminal SPFE.
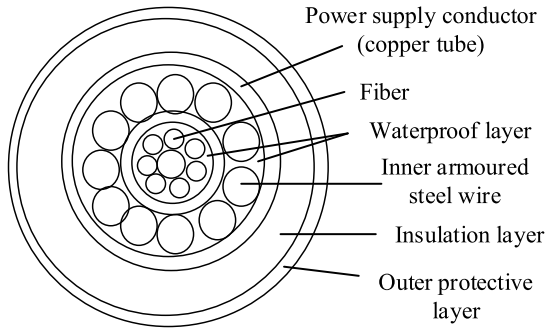

FIGURE 14. The structure diagram of the Zhongtian SOFC-LW submarine cable.

The fault location can be accurately located by analyzing the change of the system return circuit after the fault.

IV. MODELING SIMULATION AND ANALYSIS OF THE SHORT-CIRCUIT GROUNDING HIGH-IMPEDANCE FAULT LOCATION FOR A CONSTANT CURRENT REMOTE POWER SUPPLY SYSTEM

Based on the typical two-terminal 10-node mesh topology depicted in Figure 4, a system model is used to simulate and analyze various high-impedance faults. The length of the submarine cable section between the PNs is designed to be 50 km.

The electric parameters of the cable for the CUINs have international standards. Although there are some minor differences, the design concept and technology are basically the same. This paper takes SOFC-LW cable produced by Zhongtian Class Cable Company Ltd. [14] as the example to research. This type of submarine cable is widely used in the world and has a certain representative significance.

The cable structure is shown in Figure 14. As shown in Figure 1, the power supply conductor (copper pipe) of the

TABLE 1. The parameters of Zhongtian SOFC-LW submarine cable.

Parameters	Specifications
Inner Diameter of Central Steel Tube a	1.5 mm
Equivalent outer diameter of steel pipe b	4.7 mm
External Diameter of Copper Tube c	5.2 mm
Insulation outer diameter d	8.75 mm

cable and the inner armoured steel wire are in contact with each other.

When the current is applied to the copper pipe, it is inevitable that the current will flow through the steel wire and the central steel pipe.

Therefore, when establishing the model of submarine cable transmission line, it is necessary to take copper pipe, steel wire and central steel pipe as a whole to calculate the distributed inductance, capacitance and resistance of the mixed conductor. The parameters of Zhongtian SOFC-LW submarine cable are shown in Table 1.

The total flux of submarine cable can be calculated;

$$
\begin{aligned}
\varphi_{cable} &= \varphi_{core} + \varphi_{cu} \\
&= \frac{\mu_{st} i_{st}}{2\pi} \left[\frac{b^2 - 3a^2}{4(b^2 - a^2)} + \frac{a^4}{(b^2 - a^2)^2} \ln \frac{b}{a} \right] \\
&+ \mu_{cu} \frac{i_{st}}{2\pi} \ln \frac{c}{b} + \mu_{ins} \frac{i_{st}}{2\pi} \ln \frac{d}{c} + \frac{\mu_{cu} i_{cu}}{2\pi} \\
&* \left[\frac{c^2 - 3b^2}{4(c^2 - b^2)} + \frac{b^4}{(c^2 - b^2)^2} \ln \frac{c}{b} \right] + \mu_{ins} \frac{i_{cu}}{2\pi} \ln \frac{d}{c}
\end{aligned}
\tag{34}
$$

where, i_{st} is the current in the equivalent steel pipe conductor composed of central steel pipe and inner armoured steel wire; i_{cu} is the current in copper pipe; μ_{st} is the permeability of steel, μ_{cu} is the permeability of copper; μ_{ins} is the permeability of insulating layer; a is the inner diameter of the central steel pipe; b is the equivalent outer diameter of the steel pipe (also the inner diameter of the copper pipe); c is the outer diameter of the copper pipe (also the inner diameter of the insulating layer); d is the outer diameter of the insulating layer.

As shown in Table 1, the parameters of (34) can be obtained;

$$
\begin{cases}
\mu_{st} = 6.2832 \times 10^{-5} \text{N} \cdot \text{A}^{-2} \\
\mu_{cu} = 4\pi \times 10^{-7} \text{N} \cdot \text{A}^{-2} \\
\mu_{ins} = 1.6262 \times 10^{-9} \text{N} \cdot \text{A}^{-2}
\end{cases}
\tag{35}
$$

Substituting (35) into (34), we can obtain;

$$
\varphi_{cable} = 2.1004 \times 10^{-6} i_{st} + 6.5347 \times 10^{-9} i_{cu} \tag{36}
$$

$i_{st} = 0.25 i_{cable}$ and $i_{cu} = 0.75 i_{cable}$ are known, and i_{st} and i_{cu} is substituted into (36);

$$\varphi_{cable} = 5.3 \times 10^{-7} i_{cable} \quad (37)$$

The distributed inductance per unit length of the cable is;

$$L = \frac{\varphi_{cable}}{i_{cale}} \approx 0.5 \ \mu H/m \quad (38)$$

The capacitance of insulation layer of Zhongtian SOFC-LW submarine cable ε is $2.036 \times 10^{-11} C^2 \cdot m^{-2} \cdot N^{-1}$, $d = 8.75$ mm, $c = 5.2$ mm, and the distributed capacitance per unit length of the cable is;

$$C = \frac{2\pi \varepsilon}{\ln(d/c)} \approx 0.24 \ nF/m \quad (39)$$

The equivalent steel pipe and copper pipe composed of the central steel pipe and the inner armoured steel wire of the cable can be regarded as two parallel conductors, thus, the resistance of the mixed conductor composed of the equivalent steel pipe and copper pipe is equal to their parallel resistance. According to the calculation formula of the parallel resistance, the equivalent resistance of the mixed conductor per unit length can be obtained;

$$R_{\mathrm{mix}} = \frac{R_{core} R_{cu}}{R_{core} + R_{cu}} \quad (40)$$

The steel wire resistivity ρ_{st} is $2.0499 \times 10^{-7} \Omega \cdot m$ and the copper tube resistivity ρ_{cu} is $1.7243 \times 10^{-8} \Omega \cdot m$, thus, then we can obtain;

$$\begin{cases} R_{st} = R_{core} \\ \quad = \dfrac{\rho_{st}}{\pi(b^2 - a^2)} = 3.3 \times 10^{-3} \Omega/m \\ R_{cu} = \dfrac{\rho_{cu}}{\pi(c^2 - b^2)} = 1.1 \times 10^{-3} \Omega/m \end{cases} \quad (41)$$

Substituting (41) into (40), we can obtain;

$$R_{\mathrm{mix}} \approx 1 \times 10^{-3} \ \Omega/m \quad (42)$$

From the above deduction, when each cable is set to 50 km, the parameters of each link cable can be set, the equivalent resistance R_{cable} is assumed as 50 Ω, the equivalent inductance L_0 is assumed to be 25 mH, and the equivalent capacitance C_0 is assumed to be 12 uF.

It is assumed that the output current of the constant current remote supply system is I_{out} 1.5A, and the equivalent load R_{load} of the equipment node is 100 Ω. In practice, because the voltage sensor and the equivalent impedance of the submarine cable have measurement and estimation calculation errors, the data is also transmitted in the switching device and the transmission device. Therefore, the upper limit threshold of the measured average error can be set. To simulate the fluctuation in the SPFE output current or the error in the measured voltage value, an error vector matrix C is added during the operation of the remote power supply system, which satisfies the Gaussian normal distribution with a mathematical expectation of 0 and a variance of 0.045 [29], [36].
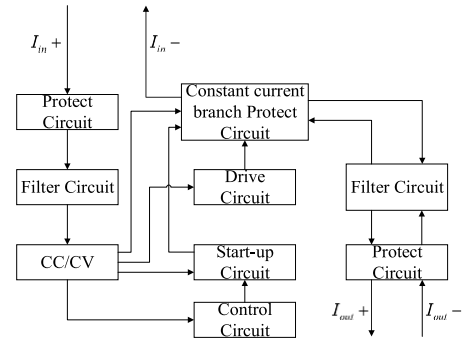

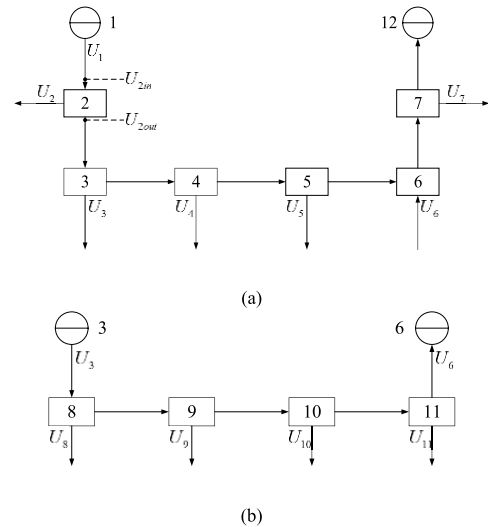**FIGURE 15.** Circuit diagram of the CC/CC convertor.

FIGURE 16. Schematic diagram of the link equivalent circuit in constant current remote power supply system. (a) The equivalent circuit of *Link* I. (b) Equivalent circuit of *link* II.

The junction box of the PN is a good conductor and the contact area with the seawater is large. Therefore, when the PN on the trunk link has a short-circuit grounding fault, the equivalent resistance value at the fault can be equivalent to zero. Meanwhile, when the PN is grounded, all the power devices in the PN cannot obtain useful power, the device cannot work normally, and the data transmission will also terminate. Thus, the fault in the PN can be diagnosed by the SS through the PMACS and CMACS. When a short-circuit grounding fault occurs in a branch, the transmission link of the branch is interrupted, the data is lost, and the load power changes, which can be measured by the CMACS and PMAS of the system. Therefore, there is no need for redundant equipment to analyze and locate the fault in the PN.

The CC/CC converter, which makes up the PNs, has an electrical isolation circuit illustrated in Figure 15. Hence, the mesh topology constant current remote power supply system can be divided into two equivalent ring links for the analysis.

Both SPFEs and PNs are equivalent to nodes in the link, and the equivalent circuit of the system link is shown in Figure 16. *Node*-1, *Node*-2, *Node*-7, and *Node*-12 form the trunk link, *Link* I consisting of *Node*-3 to *Node*-6 is depicted

TABLE 2. Equivalent values of field currents at each PN before and after short-circuit faults in PN-1 and PN-2 in the Laplace transform domain.

| Current Equivalent	I_{PN1}	I_{PN2}	I_{PN3}	I_{PN4}	I_{PN5}	I_{PN6}	I_{PN7}	I_{PN8}	I_{PN9}	I_{PN10}
Normal operation	1.523	1.499	1.498	1.464	1.546	1.494	1.468	1.561	1.490	1.473
100 Ω fault	0.187	0.162	1.150	1.383	1.387	1.386	1.443	1.461	1.492	1.536
200 Ω fault	0.107	0.062	0.935	1.115	1.185	1.285	1.494	1.508	1.479	1.539
500 Ω fault	0.011	0.092	0.629	0.771	0.900	1.071	1.450	1.557	1.530	1.497
1k Ω fault	0.028	0.027	0.415	0.533	0.620	0.814	1.569	1.521	1.491	1.528
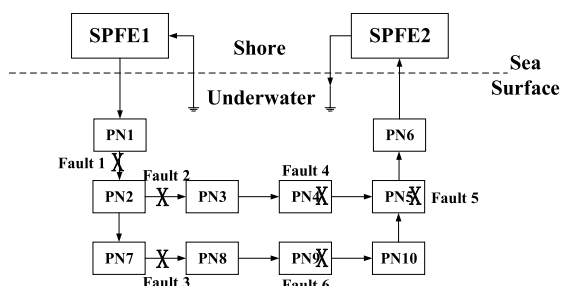
FIGURE 17. model of the system short-circuit grounding high-impedance fault.

in Figure 16(a), and *Node*-3, *Node*-6, and *Node*-8 to *Node*-11 form *Link* II, the output voltage of *Node*-3 U_3 and *Node*-6 U_6 in *Link* I are the equivalent input power for *Link* II as shown in Figure 16(b). *Node*-1 and *Node*-12 are power nodes, *Node*-3 and *Node*-6 are the branch nodes, whereas the rest are equipment nodes.

In the simulation, 3 kinds of cable faults in the CUINs are designed and basically summarize short-circuit grounding high-impedance faults that may occur in the CUINs, as shown in Figure 17.

Based on the simulation model illustrated in Figure 17, the fault location analysis of 3 kinds of faults on trunk is determined. The *Fault* 1 is the fault in the trunk cable section between PN-1 and PN-2 on *Link* I; the *Fault* 2 is the short-circuit grounding high-impedance fault occurring in the submarine cable section between PN-2 and PN-3 on *Link* I; and the *Fault* 3 is the short-circuit grounding high-impedance fault occurring in the submarine cable section between PN-7 and PN-8 on *Link* II. Assuming that the fault point *f* is located on the cable section, 25 km away from the adjacent PNs, the equivalent resistance values of the fault point are 100, 200, 500, and 1k Ω, respectively.

A. ANALYSIS OF CABLE SHORT-CIRCUIT GROUND-ING HIGH-IMPEDANCE FAULT BETWEEN PN-1 AND PN-2

Combining (20) to (23), the current equivalent of each PN before and after the submarine cable fault between PN-1 and PN-2 in the trunk cable in the Laplace transform domain is derived, as shown in Table 2.

As shown in Figure 18(a) and (b), in the Laplace transform domain, the current equivalent of all PNs is significantly lower than the normal operating status because of fault

shunt. The changes of the current equivalents in the adjacent PN-1 and PN-2 are the largest. Because of the different distance between each PN and the fault point, the corresponding equivalent resistance value R_{m-f} is different. Furthermore, the current change from PN-2 to the right-terminal SS decreases and tends to be stable that short-circuit grounding high-impedance fault in PN-1 and PN-2 can be diagnosed.

B. ANALYSIS OF THE CABLE SHORT-CIRCUIT GROUND-ING HIGH-IMPEDANCE FAULT BETWEEN PN-2 AND PN-3

Similarly, the current equivalent value of short-circuit grounding high-impedance fault in the submarine cable section between PN-2 and PN-3 in the Laplace transform domain can be simulated, as shown in Table 3.

As shown in Figure 19(a) and (b), the current equivalents of PN-2 and PN-3 in the Laplace transform domain are most pronounced and far below the normal operating status. The current equivalent values of PN-1, PN-4 to PN-6, and PN-7 to PN-10 are lower than the normal working status, but tend to be stable. From the recovery upward trend, the current between PN-2 and PN-3 changes significantly. Therefore, it is possible to diagnose short-circuit grounding high-impedance fault in the interval between PN-2 and PN-3.

C. ANALYSIS OF CABLE SHORT-CIRCUIT GROUND-ING HIGH-IMPEDANCE FAULT BETWEEN PN-7 AND PN-8

To prove that the diagnostic and interval location scheme is applicable to the short-circuit grounding high-impedance fault status of all links in the system and that it is different from the cable faults on the *Link* I and the trunk line, and using the short-circuit grounding high-impedance fault in the PN-7 and PN-8 submarine cable section on *Link* II as an example, the simulation and analysis were conducted. The equivalent values in the Laplace transform domain before and after the current fault are shown in Table 4.

As shown in Figure 20(a) and (b), the current equivalents of PN7 and PN8 in the Laplace transform domain are most pronounced and far below the normal operating conditions.

From PN-7 and PN-8 to the two-terminal SS, the current equivalent value of each PN rises slowly, restores the constant current characteristics. In addition, the current between PN-7 and PN-8 changes significantly, so it can diagnose
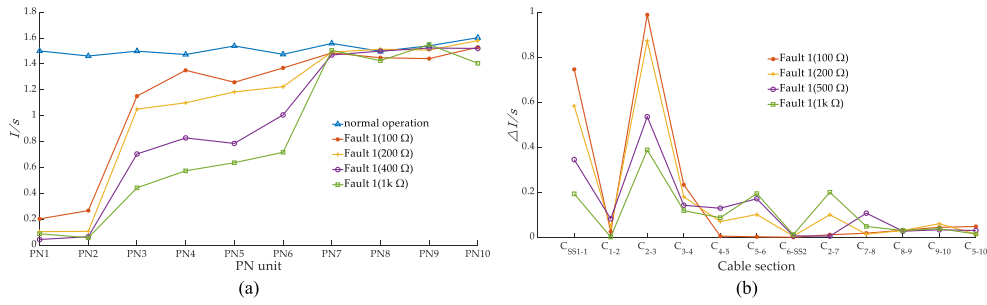
FIGURE 18. Schematic diagram of the short-circuit fault current of submarine cable between PN-1 and PN-2. (a) The distribution of current in the Laplace transform domain before and after *fault* 1. (b) The distribution of the change values of the current of each cable section in the Laplace transform domain before and after *fault* 1.

TABLE 3. Equivalent values of the field currents at each PN before and after short-circuit faults in PN-2 and PN-3 in the Laplace transform domain.

| Current Equivalent	I_{PN1}	I_{PN2}	I_{PN3}	I_{PN4}	I_{PN5}	I_{PN6}	I_{PN7}	I_{PN8}	I_{PN9}	I_{PN10}
Normal operation	1.508	1.454	1.543	1.514	1.506	1.523	1.512	1.458	1.493	1.493
100 Ω fault	1.176	0.376	0.261	0.933	1.118	1.260	1.491	1.488	1.569	1.489
200 Ω fault	0.952	0.239	0.223	0.690	0.861	1.147	1.493	1.512	1.488	1.520
500 Ω fault	0.685	0.015	0.028	0.356	0.568	0.861	1.501	1.364	1.479	1.556
1k Ω fault	0.381	0.079	0.053	0.222	0.376	0.548	1.496	1.572	1.504	1.502
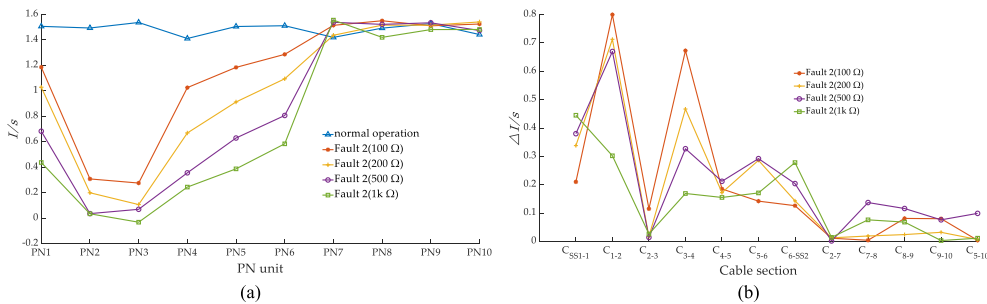
FIGURE 19. Schematic diagram of the short-circuit fault current of the submarine cable between PN-2 and PN-3. (a) Distribution of the current in the Laplace transform domain before and after *fault* 2. (b) The distribution of the change values of current of each cable section in the Laplace transform domain before and after *fault* 2.

TABLE 4. Equivalent values of field currents at each PN before and after short-circuit faults in PN-7 and PN-8 in the Laplace transform domain.

Current Equivalent	I_{PN1}	I_{PN2}	I_{PN3}	I_{PN4}	I_{PN5}	I_{PN6}	I_{PN7}	I_{PN8}	I_{PN9}	I_{PN10}
Normal operation	1.524	1.582	1.398	1.538	1.514	1.441	1.480	1.515	1.661	1.624
100 Ω fault	1.439	1.636	1.532	1.497	1.532	1.490	0.294	0.367	1.018	1.213
200 Ω fault	1.530	1.445	1.532	1.573	1.522	1.546	0.199	0.153	0.713	0.893
500 Ω fault	1.539	1.448	1.451	1.463	1.367	1.565	0.085	0.037	0.450	0.513
1k Ω fault	1.495	1.489	1.514	1.514	1.461	1.498	0.029	0.065	0.272	0.417

short-circuit grounding high-impedance fault in the interval between PN-7 and PN-8.

It is assumed that the fault points are respectively located on the submarine cable section, the adjacent left-terminal PN is 10, 25, and 40 km, and the equivalent resistance value of the fault point is set to 100 Ω. By combining (28), (32), and (33), we can calculate the location of short-circuit grounding high-impedance fault point and the equivalent resistance value at the fault. The results are shown in Table 5.
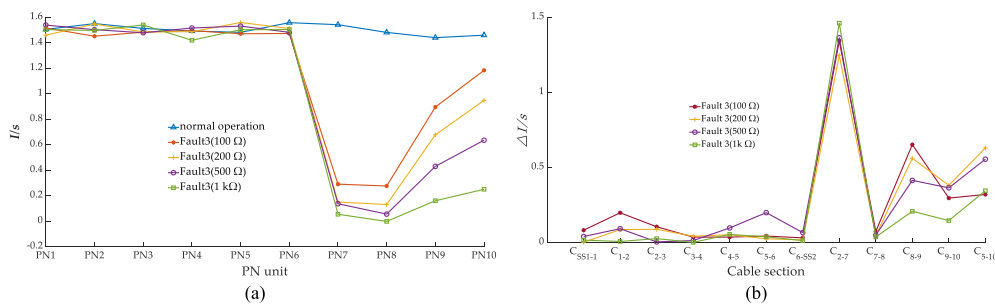
FIGURE 20. Schematic diagram of the short-circuit fault current of the submarine cable between PN-7 and PN-8. (a) The distribution of the current in the Laplace transform domain before and after *fault* 3. (b) The distribution of the change values of the current of each cable section in the Laplace transform domain before and after *fault* 3.

TABLE 5. Analysis data of the fault location in the different links.

Status	Fault 1	Fault 2	Fault 3
10 km Analysis results /km	10.074	9.852	9.550
Error /km	0.074	-0.148	0.45
25 km Analysis results /km	25.044	25.016	25.009
Error /km	0.044	0.016	0.009
40 km Analysis results /km	40.52	40.257	40.430
Error /km	0.52	0.257	0.430

TABLE 6. Analysis data of the fault resistance in different links.

Status	Fault 1	Fault 2	Fault 3
100 Ω Analysis results /Ω	99.498	100.046	99.977
Error /Ω	-0.503	0.046	-0.023
200 Ω Analysis results /Ω	199.937	200.052	201.009
Error /Ω	-0.063	0.052	1.009
500 Ω Analysis results /Ω	499.717	500.241	500.029
Error /Ω	-0.283	0.241	0.029
1k Ω Analysis results /Ω	999.012	1000.855	1000.089
Error /Ω	-0.988	0.855	0.089

As shown in Table 5, the measurement error is substituted into the system simulation. The analysis can obtain 3 fault conditions, and the fault location error is within 0.6 km. This shows good fault location capability for submarine cable faults.

In summary, the simulation analysis of 3 kinds of fault conditions can be obtained. By designing a classic model of the two-terminal 10-node mesh topology constant current remote power supply system in CUINs, the short-circuit grounding high-impedance faults in different links are simulated, while the voltage distribution and variation differences in the Laplace transform domain before and after the short-circuit grounding high-impedance fault are analyzed and compared, and the location of the fault is analyzed and calculated. It was verified that the proposed fault diagnosis and location method can clearly and accurately determine the fault condition and locate the fault point. This further proves that the short-circuit grounding high-impedance fault caused by bending or the power supply conductor tearing in the underwater constant current remote supply system can be diagnosed, which provides a technical method for future operation and maintenance of the system.

According to the system fault simulation model in Figure 17, the simulation of 3 different faults is conducted for the detection of the equivalent resistance of the fault point. Supposing that the fault point in case of a fault in the middle of 3 kinds of cable sections, the distance between adjacent PNs is 25 km and the equivalent resistance value of the fault point is assumed 100, 200, 500, and 1k Ω. The equivalent resistance value analysis at the fault was performed according

to the simulation calculation contents in (33), and the results are shown in Table 6.

As shown in Table 6, the error in the analysis and calculation of the 3 kinds of faults is within ±1.1 Ω, which provides a certain ability to locate the fault of the submarine cable.

The four fault resistance values have been set (100, 200, 500, and 1k Ω), which basically covers the occurrence status of short-circuit grounded high-impedance faults. According to (23), (27) and Figure 18 to Figure 20, when the fault occurs, the fault can be diagnosed, and there is a certain regularity in the current change in the Laplace transform domain after the underwater fault occurs, as shown in Figure 18 to Figure 20. In the CUINs, the current information can be collected by the PMACS and compared with the theoretical simulation results to diagnose whether the constant current remote supply system has faults. When the fault is determined to exist, the SPFE supplied the power for underwater system individually from both terminals, according to (33), the fault location is determined by calculating the shunt loss of the current in the trunk before and after the fault, the simulation results of equivalent resistance values of the fault are shown in Table 6. The simulation results show that the equivalent resistance of the fault obtained by this method is basically the same as the theoretical value. The proposed method is feasible and has a certain positioning function.

In summary, the simulation analysis of the three open-circuit fault conditions is possible. By simulating short-circuit grounding high-impedance faults in different

links, the calculation and analysis of the fault point resistance values are obtained. It is also verified that the proposed fault diagnosis and positioning method can clearly and accurately determine the short-circuit ground fault condition and locate the fault point and this additionally proves that the method of bidirectionally detecting the trunk current shunt loss through the SS can accurately locate the grounding high-impedance fault point and calculate the equivalent resistance value of the fault point. Finally, it is suitable for the detection, location and isolation of open-circuit faults in constant current remote power supply systems of CUINs.
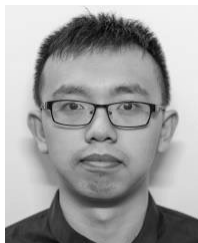
V. CONCLUSION

With the continuous development of cabled underwater information networks, detection, location, and isolation of faults in remote power supply systems has become an important part of system operation and maintenance. According to the equivalent theorem of the Norton current source, this paper diagnoses the short-circuit grounding high-impedance fault status by analyzing the variation difference of the equivalent current in the Laplace transform domain; locates the fault location by calculating the shunt loss of the current in the trunk before and after the fault; and based on the model of the two-terminal 10-node mesh topology constant current remote power supply system, the modeling and simulation verifies the rationality and feasibility of the method. Currently, this method is still in the theoretical stage, and the range that the current method can be used to locate is still relatively large. To verify the rationality of this method designed, the next step would be to eliminate the influence of the measurement error, improve the positioning accuracy, establish an optimized model and build a mesh topology remote power supply system prototype physical test platform. We can then further verify the practical application performance of the method through experiments. In addition, a design the corresponding controller would lay the foundation for the standardization and systemization of the CMACS and PMACS in the cabled underwater information network.

REFERENCES

[1] Y. Chen, *Fundamentals of Ocean Technology*. Beijing, China: Ocean Press, 2018, pp. 227–235.

[2] F. Lu, H. Zhou, X. Peng, J. Yue, and P. Wang, "Technical preparation and prototype development for long-term cabled seafloor observatories in Chinese marginal seas," in *Seafloor Observatories*. Berlin, Germany: Springer, 2015, ch. 19, pp. 503–529.

[3] L. Carter, "Environmental impacts," in *Submarine Cables and the Oceans: Connecting the World*. London, U.K.: Lavenham Press, 2009, ch. 5, pp. 29–37.

[4] R. Diamant and L. Lampe, "Low probability of detection for underwater acoustic communication: A review," *IEEE Access*, vol. 6, pp. 19099–19112, 2018.

[5] F. Lü and H. Zhou, "Progress of scientific cabled seafloor observatory networks," *J. Eng. Stud.*, vol. 8, pp. 139–154, Feb. 2016.

[6] Z. Gao and G. Guo, "Fixed-time leader-follower formation control of autonomous underwater vehicles with event-triggered intermittent communications," *IEEE Access*, vol. 6, pp. 27902–27911, 2018.

[7] K. D. LePage, G. Canepa, J. Bates, A. Tesei, M. Micheli, and A. Munafo, "Bistatic continuous active sonar processing using arrays towed from unmanned underwater vehicles," *J. Acoust. Soc. Amer.*, vol. 141, no. 5, p. 3850, May 2017.

[8] W. Gan, D. Zhu, and D. Ji, "QPSO-model predictive control-based approach to dynamic trajectory tracking control for unmanned underwater vehicles," *Ocean Eng.*, vol. 158, pp. 208–220, Jun. 2018.

[9] K. Hu, Z. Guo, G. Ma, W. Zhou, and Z. Sun, "Complex virtual instrument model for ocean sensor networks," *IEEE Access*, vol. 6, pp. 21934–21944, 2018.

[10] M. Best and A. Purser, "Deep sea shell taphonomy: Interactive benthic experiments in hydrate environments of barkley canyon, ocean networks Canada," *Plant J.*, vol. 55, no. 5, pp. 746–759, Apr. 2015.

[11] W. Pinxian, "Seafloor observatories: The third platform for Earth system observation," *Chin. J. Nature*, vol. 29, no. 3, pp. 125–130, Jul. 2007.

[12] C. Hua, "Technologies of cabled submarine networking observation," in *International Progress in Submarine Scientific Observation*. Shanghai, China: Tongji Univ. Press, 2017, ch. 9, pp. 139–154.

[13] J. Chesnoy, "Terminal equipment," in *Undersea Fiber Communication Systems*, 2nd ed. San Diego, CA, USA: Academic, 2016, ch. 10, pp. 237–260.

[14] X. Zhou, C. Fan, D. Li, and Y. Zhou, "Power scheme selecting method for constant current power system of cabled seafloor observatory network," *Autom. Electric Power Syst.*, vol. 39, no. 19, pp. 126–131, Oct. 2015.

[15] Y. Chen, B. M. Howe, and C. Yang, "Actively controllable switching for tree topology seafloor observation networks," *IEEE J. Ocean. Eng.*, vol. 40, no. 4, pp. 993–1002, Oct. 2015.

[16] M. A. El-Sharkawi, A. Upadhye, S. Lu, H. Kirkham, B. M. Howe, T. McGinnis, and P. Lancaster, "North east pacific time-integrated undersea networked experiments (NEPTUNE): Cable switching and protection," *IEEE J. Ocean. Eng.*, vol. 30, no. 1, pp. 232–240, Jan. 2005.

[17] C. R. Barnes, M. M. R. Best, F. R. Johnson, L. Pautet, and B. Pirenne, "Challenges, benefits, and opportunities in installing and operating cabled ocean observatories: Perspectives from NEPTUNE Canada," *IEEE J. Ocean. Eng.*, vol. 38, no. 1, pp. 144–157, Jan. 2013.

[18] S. Monna, G. Falcone, L. Beranzoli, F. Chierici, G. Cianchini, M. De Caro, A. De Santis, D. Embriaco, F. Frugoni, G. Marinaro, C. Montuori, L. Pignagnoli, E. Qamili, T. Sgroi, and P. Favali, "Underwater geophysical monitoring for European multidisciplinary seafloor and water column observatories," *J. Mar. Syst.*, vol. 130, pp. 12–30, Feb. 2014.

[19] Y.-H. Chen, C.-J. Yang, D.-J. Li, B. Jin, and Y. Chen, "Study on 10 kVDC powered junction box for a cabled ocean observatory system," *China Ocean Eng.*, vol. 27, no. 2, pp. 265–275, 2013.

[20] J.-K. Choi, S. Nishida, T. Yokobiki, and K. Kawaguchi, "Automated cable-laying system for thin optical-fiber submarine cable installation," *IEEE J. Ocean. Eng.*, vol. 40, no. 4, pp. 981–992, Oct. 2015.

[21] J. K. Choi, T. Yokobiki, and K. Kawaguchi, "ROV-based automated cable-laying system: Application to DONET2 installation," *IEEE J. Ocean. Eng.*, vol. 43, no. 3, pp. 665–676, Jul. 2017.

[22] A. Aboulian, D. H. Green, J. F. Switzer, T. J. Kane, G. V. Bredariol, P. Lindahl, J. S. Donnal, and S. B. Leeb, "NILM dashboard: A power system monitor for electromechanical equipment diagnostics," *IEEE Trans. Ind. Informat.*, vol. 15, no. 3, pp. 1405–1414, Mar. 2019.

[23] H. Tayama, O. Fukuda, K. Yamamoto, Y. Inoue, and Y. Koike, "6.6 kV XLPE submarine cable with optical fiber sensors to detect anchor damage and defacement of wire armor," *IEEE Trans. Power Del.*, vol. 10, no. 4, pp. 1718–1723, Oct. 1995.

[24] T. Nishimoto, T. Miyahara, H. Takehana, and F. Tateno, "Development of 66 kV XLPE submarine cable using optical fiber as a mechanical-damage-detection-sensor," *IEEE Trans. Power Del.*, vol. 10, no. 4, pp. 1711–1717, Oct. 1995.

[25] M. A. Farahani and T. Gogolla, "Spontaneous Raman scattering in optical fibers with modulated probe light for distributed temperature Raman remote sensing," *J. Lightw. Technol.*, vol. 17, no. 8, pp. 1379–1391, Aug. 1999.

[26] J. C. Juarez, E. W. Maier, K. N. Choi, and H. F. Taylor, "Distributed fiber-optic intrusion sensor system," *J. Lightw. Technol.*, vol. 23, no. 6, pp. 2081–2087, Jun. 2005.

[27] M. Natu and A. S. Sethi, "Probe station placement for fault diagnosis," in *Proc. IEEE Global Telecommun. Conf.*, Washington, DC, USA, Nov. 2007, pp. 113–117.

[28] S. Wei, Y. Zhou, and Y. Huang, "Synchronous motor-generator pair to enhance small signal and transient stability of power system with high penetration of renewable energy," *IEEE Access*, vol. 5, pp. 11505–11512, 2017.

[29] Z. Lou, D. Shen, and Y. Wang, "Preliminary-summation-based principal component analysis for non-Gaussian processes," *Chemometrics Intell. Lab. Syst.*, vol. 146, pp. 270–289, Aug. 2015.

[30] Y. Wang, Y. Si, B. Huang, and Z. Lou, "Survey on the theoretical research and engineering applications of multivariate statistics process monitoring algorithms: 2008–2017," *Can. J. Chem. Eng.*, vol. 96, no. 10, pp. 2073–2085, Oct. 2018.

[31] S. Lu and M. A. El-Sharkawi, "NEPTUNE power system: Detection and location of switch malfunctions and high impedance faults," in *Proc. IEEE Int. Symp. Ind. Electron.*, Montreal, QC, Canada, Jul. 2006, pp. 1960–1965.

[32] T. Chan, C.-C. Liu, B. M. Howe, and H. Kirkham, "Fault location for the NEPTUNE power system," *IEEE Trans. Power Syst.*, vol. 22, no. 2, pp. 522–531, May 2007.

[33] Z.-F. Zhang, Y.-H. Chen, D.-J. Li, B. Jin, C.-J. Yang, and J. Wang, "Use of a coded voltage signal for cable switching and fault isolation in cabled seafloor observatories," *Frontiers Inf. Technol. Electron. Eng.*, vol. 19, no. 11, pp. 1328–1339, Nov. 2018.

[34] F. Lü, H. Zhou, J. Yue, and B. He, "Remote power monitoring and control system for cabled seafloor observatory networks," *Tongji Daxue Xuebao/J. Tongji Univ.*, vol. 42, no. 11, pp. 1725–1732, Nov. 2014.

[35] F. Lu, H. Zhou, J. Yue, and H. Bin, "Power system reliability of networks structure and cabled seafloor topology observatory," *J. Tongji Univ.*, vol. 42, no. 10, pp. 1604–1610, Oct. 2014.

[36] Y. Feng, Z. Li, X. Wang, Z. He, and L. Pan, "Open-circuit fault identification and section locating method of optoelectric cable of seafloor observatory network," *Dianli Xitong Zidonghua/Automat. Electr. Power Syst.*, vol. 39, no. 10, pp. 151–156, May 2015.

[37] Z. Zhang, Y. Chen, D. Li, B. Jin, C. Yan, and F. Xu, "An active node switching method based on discrete-voltage intervention for seafloor observation network," *Mar. Technol. Soc. J.*, vol. 51, no. 3, pp. 48–59, May 2017.

[38] S. Zheng and F. Lyu, "Switching high voltage DC power in branching units of large-scale cabled seafloor observatories," in *Proc. 5th Int. Conf. Coastal Ocean Eng.*, Shanghai, China, 2018, pp. 1–7.

[39] F. Zhang, B. Jin, D. Li, Y. Chen, C. Yang, and H. Yang, "Study on the short fault isolation of cabled ocean observatory," in *Proc. MTS/IEEE TECHNO-OCEANS Conf.*, Monterey, CA, USA, Sep. 2016, pp. 1–5.

[40] J. Chen, X. Su, X. Zhang, C. Choi, and D. Choi, "A survey on ocean observatory networks," in *Proc. Conf. Res. Adapt. Convergent Syst.*, Honolulu, HI, USA, 2018, pp. 126–131.

[41] D. W. Harris and F. K. Duennebier, "Powering cabled ocean-bottom observatories," *IEEE J. Ocean. Eng.*, vol. 27, no. 2, pp. 202–211, Apr. 2002.

[42] Z. Zhang, X.-J. Zhou, X.-C. Wang, and Y.-Y. Zhou, "Short-circuit fault diagnosis and interval location method for constant current remote supply system in cabled underwater information networks," *J. Zhejiang Univ. (Eng. Science)*, vol. 53, no. 6, pp. 1190–1197, Jun. 2019.

XUEJUN ZHOU was born in Wuwei, China, in 1962. He received the B.Eng. degree from Xidian University, Xi'an, China, in 1984, the M.Eng. degree in communication and electronic system from the PLA University of Science and Technology, Nanjing, China, in 1988, and the Ph.D. degree in communication engineering from the National University of Defense Technology, Changsha, China, in 2003.

From 1996 to 2001, he was an Associate Professor with the Naval College of Electronic Engineering. He has been a Professor with the College of Electronic Engineering, Naval University of Engineering, since 2002. He has been the Chief Professor of the Department of Information Network Engineering, NUE, since 2015. He holds four patents. He is the author of two books and more than 110 articles. His research interests include underwater cabled optical communication, quantum secure communication, and underwater remote power supply systems.

XICHEN WANG received the B.Eng. and M.Eng. degrees in communication engineering from the Naval University of Engineering (NUE), Wuhan, China, in 2009, and the Ph.D. degree in communication and information systems from the NUE, in 2015.

Since 2015, he has been a Lecturer with the College of Electronic Engineering, NUE. He was responsible for the Youth Project of the Natural Science Foundation of Hubei Province. He has participated in the National Natural Science Foundation of China (NSFC) and military research projects for many times, and charged and taken part in the power supply laboratory prototype system construction of the cabled underwater information network. His research interests include fiber optics, underwater cabled optical communication, and underwater remote power supply systems.

ZHENG ZHANG received the B.Eng. degree from Hohai University (HHU), Nanjing, China, in 2014, and the M.Eng. degree from Naval University of Engineering (NUE), Wuhan, China, in 2016, where he is currently pursuing the Ph.D. degree. His research interests include fiber optics, underwater cabled optical communication, and underwater remote power supply systems. Since 2015, he has been participated in the National Natural Science Foundation of China (NSFC) and military research projects for many times. He has completed the deep sea test of the constant current remote supply system equipment and the power supply laboratory prototype system construction of the cabled underwater information network.

LEI WANG received the B.Eng. degree from the Ocean University of China, Qingdao, China, in 2018. He is currently pursuing the M.Eng. degree with the Naval University of Engineering (NUE), Wuhan, China.

Since 2018, he has been participated in the power supply laboratory prototype system construction of the cabled underwater information network. His research interests include fiber optics, underwater cabled optical communication, and underwater remote power supply systems.

• • •